

Inhibition guarantees ceaseless cortex network dynamics

Daniel B. Larremore,^{1,2} Woodrow L. Shew,³ Shan Yu,⁴ Dietmar Plenz,⁴ Edward Ott,⁵ Francesco Sorrentino,⁶ and Juan G. Restrepo⁷

¹*Department of Epidemiology, Harvard School of Public Health, Boston, MA 02115, USA*

²*Center for Communicable Disease Dynamics, Harvard School of Public Health, Boston, MA 02115, USA*

³*Department of Physics, University of Arkansas, Fayetteville, AR 72701, USA*

⁴*National Institutes of Health, Section on Critical Brain Dynamics, Bethesda, MD 20817, USA*

⁵*Institute for Research in Electronics and Applied Physics,
University of Maryland, College Park, MD 20742, USA*

⁶*Department of Mechanical Engineering, University of New Mexico, Albuquerque, NM 87106, USA*

⁷*Department of Applied Mathematics, University of Colorado, Boulder, CO 80309, USA*

Proper function of diverse biological, social, and engineered networks requires a balance of competing influences. In the cerebral cortex, inhibitory neurons keep excitatory neurons in check and play a crucial role in sensory processing. Experiments suggest inhibition is required to maintain cortex network dynamics at the critical point of a phase transition at which neuronal avalanches occur, and further suggest criticality optimizes aspects of cortical information processing. We numerically and analytically investigate critical dynamics in a network model and discover a previously unappreciated consequence of inhibition: the greater the number of inhibitory nodes, the more likely network dynamics are to be intrinsically self-sustaining. In the cortex, ongoing intrinsic dynamics play a role in memory consolidation and learning. We identify critical avalanches and also predict an experimentally observable signature of criticality that we confirm with recordings from the cortex of two awake monkeys, suggesting inhibition confers both balance and ceaseless critical dynamics in the cortex.

PACS numbers: ??

Networks of excitable nodes have been successfully used to model a variety of phenomena, including reaction-diffusion systems [1], economic trade crises [2], and epidemics [3]. In neuroscience in particular, excitable network models have successfully explained experiments revealing that the mammalian cortex may operate at the critical point of a phase transition [4–6]. In this critical state, the cortex exhibits optimal dynamic range [4–7] and information capacity [1], and features cascades of activity called neuronal avalanches [1, 7, 9, 10], with experimental evidence drawn from humans [11, 12], monkeys [1, 9], cats [13], rats [14], and slices of rat cortex [1, 7, 10]. However, there remains a gap between theory and experiment: models that successfully explain all of these experimental observations so far have included only excitatory nodes. This neglects two important facts: 1) mammalian cortex contains approximately 20% inhibitory neurons [15] and 2) inhibitory neurons are crucial for maintaining critical dynamics and optimized function [1, 7, 16]. We close this gap by studying a model that includes inhibitory nodes and find an unexpected effect; adding inhibition destabilizes low activity levels, creating ceaseless network activity. Moreover, critical avalanches remain embedded within ongoing dynamics. In this Letter, we combine analytical results, simulation, and recordings from cortex of two awake monkeys to explain these phenomena. We conclude that ceaseless population activity is practically inevitable if 1) the network includes inhibitory nodes and 2) population dynamics are maintained near criticality, i.e., near balanced excitation and inhibition. Since the primary effect of inhibitory neurons is to suppress activity, it is surprising that, secondarily, they guarantee that population activity is never fully suppressed.

In the cortex, ongoing intrinsic dynamics play a role in

memory consolidation and learning [17, 18]. It is commonly believed that the cortex remains active simply because sensory input is ongoing—ceaseless stimulus causes ceaseless response. However, this point of view is challenged by experiments in which the cortex is physically isolated from sensory input (e.g., surgically [1, 7, 19, 20]), but remains active. Another possibility is that certain “pacemaker” neurons are intrinsically active even without input [21], providing a ceaseless stimulus from within the cortical network. Some analytical and modeling studies suppose that interactions among excitatory neurons result in dynamic attractors and thus persistent firing in the cortex [22, 23]. Other models generate asynchronous self-sustained activity with balanced excitation and inhibition [24–26]. However, none of these approaches provides an explanation of certain experimental observations, such as neuronal avalanches [1, 7, 9, 10] and the lack thereof when inhibition is disrupted [1, 7, 16]. A theoretical perspective that better explains these observations is that of critical phenomena (possibly self-organized) [4–7, 16, 27, 28], yet these models avoid explicit inhibitory nodes and require external stimulus. In this context our findings offer new solutions to two longstanding riddles: 1) what are the underlying mechanisms of ceaseless cortex dynamics and 2) how does competition of excitation and inhibition result in critical network dynamics?

Our model consists of a sparse network of N interacting excitable nodes. At each discrete time step t , each node n may be in one of two states $s_n(t) = 0$ or $s_n(t) = 1$, corresponding to quiescent or active respectively. When a node n is in the active state $s_n(t) = 1$, node m receives an input of strength A_{mn} . Each node n is either excitatory or inhibitory, respectively corresponding to $A_{mn} \geq 0$ or $A_{mn} \leq 0$ for all m . If

there is no connection from node n to node m , then $A_{mn} = 0$. Each node n sums its inputs at time t and passes them through a transfer function $\sigma(\cdot)$ so that its state at time $t + 1$ is

$$s_n(t + 1) = 1 \text{ with probability } \sigma \left(\sum_{m=1}^N A_{nm} s_m(t) \right), \quad (1)$$

and 0 otherwise, where the transfer function is piecewise linear; $\sigma(x) = 0$ for $x < 0$, $\sigma(x) = x$ for $0 < x < 1$, and $\sigma(x) = 1$ for $x \geq 1$. In the presence of net excitatory input, a node may become active, but in the absence of input, or in the presence of net inhibitory input, a node never becomes active.

We consider the dynamics described above on the example of networks drawn from the ensemble of directed random networks, where the probability that each node m connects to each other node n is p . In a network of N nodes, this results in a mean in-degree and out-degree of $\langle k \rangle = Np$. First, to create the matrix A , each connection strength A_{mn} is independently drawn from a distribution of positive numbers. While our analytical results hold for any distribution with mean γ , in our simulations the distribution is uniform on $[0, 2\gamma]$. Next, a fraction α of the nodes are designated as inhibitory and each column of A that corresponds to the outgoing connections of an inhibitory node is multiplied by -1 . We explored a range of $0 \leq \alpha \leq 0.3$, which includes the physiologically realistic fraction $\alpha \approx 0.2$ of inhibitory neurons in mammalian cortex [15]. The factor γ is chosen such that the largest eigenvalue λ of the matrix A is unity, which for large networks implies $\gamma \approx 1/[\langle k \rangle(1 - 2\alpha)]$. In the case where all nodes are excitatory, $\alpha = 0$, this condition ensures that the network operates at criticality [5]. Our model is similar to a previously published model, which was used to successfully explain experimental observations of neuronal avalanches [9, 10, 14, 29], cortical dynamic range [7], information transmission [1], and information capacity [1], but which lacks inhibition.

Our study focuses on the aggregate activity of the network, defined as $S(t) = N^{-1} \sum_n s_n(t)$, the fraction of nodes that are excited at time t . According to Eq. (1), if the entire network is quiescent, $S = 0$, it will remain quiescent indefinitely. We find that when there are no inhibitory nodes ($\alpha = 0$) network activity ceases after a typically short time, in agreement with previous results [4–6]. However, for sufficiently large $\alpha > 0$, we find that the lifetime of activity becomes extremely long; the state $S = 0$ is in practice never reached. By conducting simulations with various values of N , $\langle k \rangle$, and α , we found that the expected lifetime of activity after an initial excitation of 100 nodes grows approximately exponentially with increasing α , with growth rate proportional to $N/\langle k \rangle$ (Fig. 1A). Thus large, sparse networks, like the mammalian cortex, are likely to generate ceaseless activity without any external source of excitation. The expected lifetime of activity τ , derived analytically in supplementary materials (SM), is approximately given by

$$\tau = C_1 \exp \left\{ C_2 \frac{N}{\langle k \rangle} \frac{\alpha}{(1 - 2\alpha)(1 - \alpha)} \right\}, \quad (2)$$

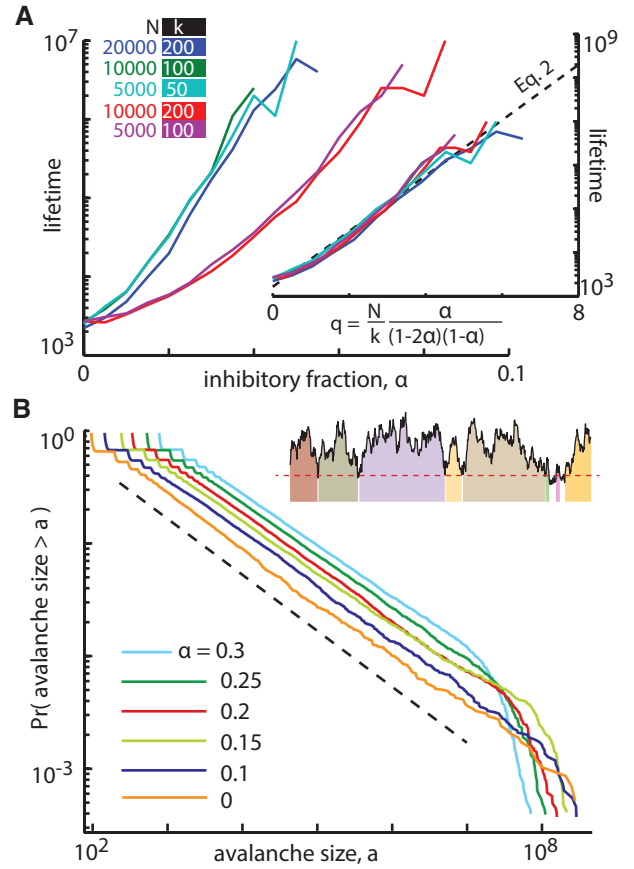


FIG. 1. (Color online.) Increasing inhibition causes ceaseless activity while maintaining criticality. **A)** Lifetime of network activity increases with inhibitory fraction α for various N and $\langle k \rangle$. Simulations began with 100 active nodes, with lifetime calculated from the fraction of simulations that ceased prior to $T = 10^4$ timesteps. (inset) Lifetime scales correctly with q , as shown in Eq. (2), indicated by collapse of curves. **B)** Probability that an avalanche size is larger than a as a function of a for various values of α . The dashed line corresponds to a size distribution $P(a) \sim a^{-3/2}$. Data are shown from simulation of $N = 10^4$ nodes over 3×10^6 timesteps.

where C_1 and C_2 are two constants. The inset for Fig. 1A shows how plots of τ for different values of $N/\langle k \rangle$ collapse when plotted as a function of $q = N\alpha/\langle k \rangle(1 - 2\alpha)(1 - \alpha)$, in agreement with Eq. (2).

Previous studies of critical neural network dynamics have focused on cascades of activity that emerge, called neuronal avalanches [9]. In some models and *in vitro* experiments [1, 7, 10, 29], such avalanches occur with well-defined beginnings and ends; given many avalanches, statistical features such as avalanche size distributions with power-law functional form are indicative of critical dynamics. In contrast, our model generates a single ceaseless cascade for cortex-like inhibition ($\alpha \approx 0.2$). Thus, at first glance, it is not clear if our model is critical and avalanche size distributions appear ill-suited to test for criticality. This same issue is faced if one attempts to assess criticality based on cortex dynamics recorded from awake animals. However, adopting an intuitive and recently introduced definition of an avalanche [12], we found power-law avalanche size distributions in both our

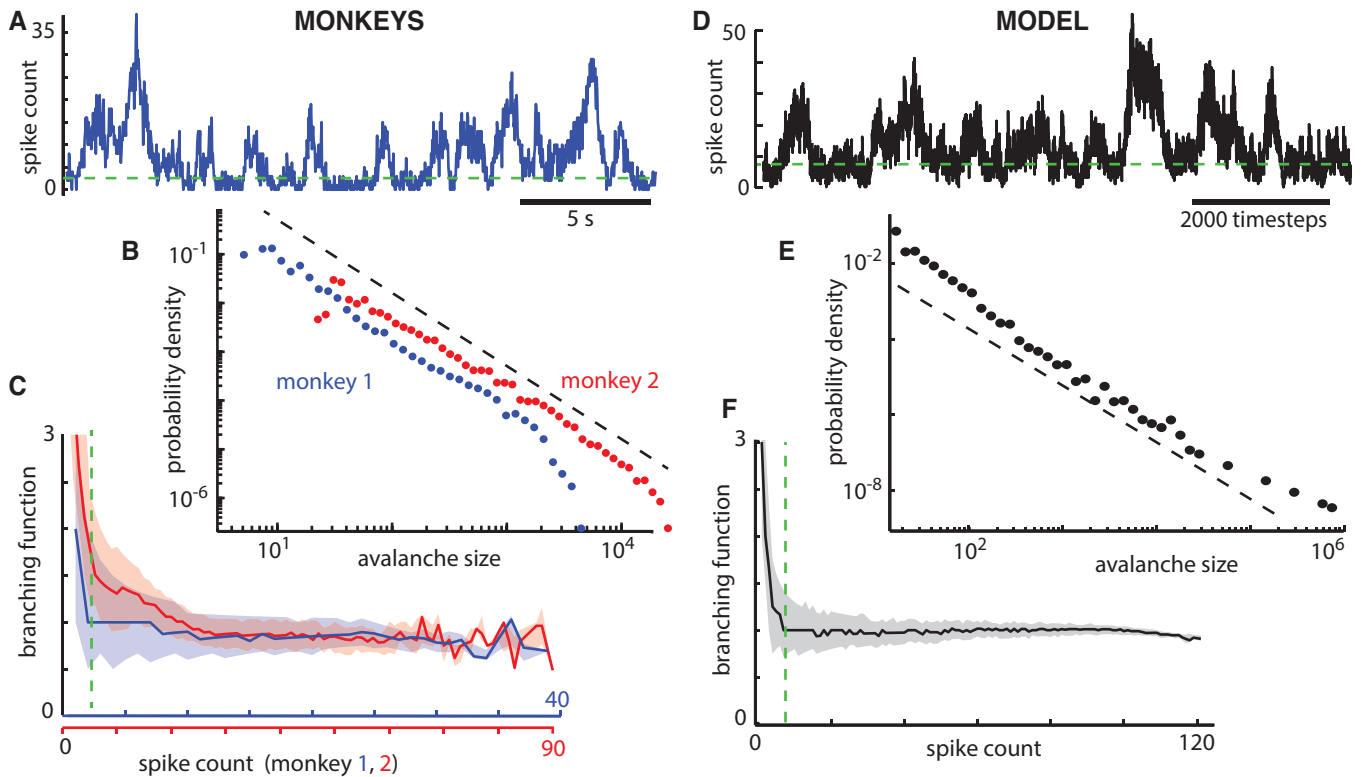


FIG. 2. (Color online.) Model and analytical predictions agree with awake monkey data. **A**) Spike-count time series recorded from premotor cortex of an awake monkey (monkey 1). (Full experimental details in SM.) Avalanches are defined as excursions above a threshold level spike count (green dashed line). **B**) Avalanche size distributions for both monkeys are close to power-law with $-3/2$ exponent (black dashed line). **C**) Empirical branching functions of both monkeys show wide critical range ($\Lambda(S) \approx 1$) that produces power-law avalanche statistics and supercritical region ($\Lambda(S) > 1$) at low S that produces self-sustained activity. Line indicates median; shaded region delineates lower and upper quartiles. As in A, green dashed line indicates threshold for avalanche calculation for Monkey 1. **D**) To fairly compare with monkeys, we generated a spike count time series by sampling only 65 of $N = 10^4$ model neurons ($\langle k \rangle = 300$, $\alpha = 0.2$). **E**) Subsampled model data avalanche size distribution is similar to monkey avalanche size distributions. (The distribution from fully sampled timeseries shows a robust power law, Fig. 1B.) **F**) Empirical branching function of the subsampled model compares well to monkey data in C.

model data (Fig. 1B) and spikes recorded from motor cortex of two awake monkeys (Fig. 2A,B). For details on monkey electrophysiology and data analysis see SM. Specifically, we define an avalanche as an excursion of $S(t)$ above a threshold level S^* , fragmenting a ceaseless timeseries of $S(t)$ into many excursions above the threshold (inset of Fig. 1B). We define the size of an avalanche as $a = \sum S(t)$, summing over the duration of the avalanche. For all α tested in the model, the avalanche sizes are power-law distributed (Fig. 1B) with exponents that are consistent with those observed in previous *in vitro* and *in vivo* experiments in mammalian cortex [9, 10] and models of critical avalanches in networks [29], with size distribution $P(a) \sim a^{-\beta}$ with $\beta \approx -1.5$. Estimated exponents from data [30] are shown in Table S1. This is equivalent to a complementary cumulative distribution function $P(\text{avalanche size} > a) \sim a^{-1/2}$ as displayed in Figure 1B. However, previous *in-vivo* and *in-vitro* studies have not defined avalanches in the way we define here. To more directly test our model, we applied our threshold-based avalanche detection scheme to spike count time series based on ongoing or single unit resting activity of two monkeys (65 units for Monkey 1, 131 units for Monkey 2; see SM). To account for possible confounding due to severely subsampling the full network of neurons,

we compared the monkey avalanche size distributions to those obtained from a subset of 65 out of the full set of $N = 10^4$ model neurons (Fig. 2). Good agreement suggests that this approach is robust to subsampling the neural population (this is further demonstrated in Figure S1).

To understand why inhibition results in ceaseless activity at criticality, we analyze the model described in Eq. (1). A central concept in our analysis is the *branching function* $\Lambda(S)$, which we define as the expected value of $S(t+1)/S(t)$ conditioned on the level of activity $S(t)$ at time t ,

$$\Lambda(S) = S^{-1} \mathbb{E}[S(t+1) | S(t) = S]. \quad (3)$$

We note that Λ is similar to the branching ratio in branching processes except that here we allow it to vary with S . Since S is unknown for the monkey data, we estimate an empirical branching function with spike count in place of S (Fig. 2C). For values of S such that $\Lambda(S) > 1$, activity will increase on average, and for values of S such that $\Lambda(S) < 1$, activity will decrease on average. The expectation in Eq. (3) is taken over many realizations of the stochastic dynamics. Noting that there is a set of many different possible configurations $\vec{s} = \{s_n\}_{n=1}^N$ of active nodes that result

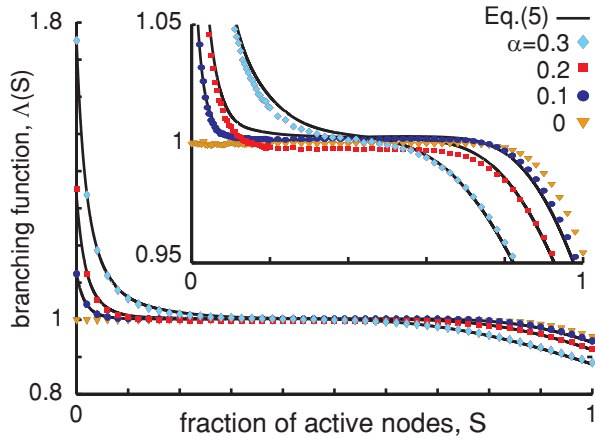


FIG. 3. (Color online.) Branching function $\Lambda(S)$ explains ceaseless and near-critical behavior. Each symbol corresponds to the average of $S(1)/S(0)$ over 10^4 repetitions of each $S(0)$ on a single network of $N = 10^4$ nodes and mean degree $\langle k \rangle = 100$. Different symbols correspond to different inhibitory fraction α ; see legend. Solid lines are predicted values given by Eq. (5). As S becomes small activity becomes biased toward growth. As S becomes large activity becomes biased toward decay. Thus S tends to be maintained near $\Lambda \approx 1$. Inset shows vertically expanded view around $\Lambda = 1$.

in the same active fraction S , we define this set as $\mathcal{S}(S)$. Thus, $\Lambda(S) = S^{-1} \mathbb{E}_{\mathcal{S}(S)} [\mathbb{E}[S(t+1) | \vec{s}(t) \in \mathcal{S}(S)]]$, where the outer expectation averages over configurations in $\mathcal{S}(S)$ and the inner expectation averages over realizations of the dynamics (1) for a given configuration. We then use Eq. (1) to write

$$\Lambda(S) = S^{-1} \mathbb{E}_{\mathcal{S}(S)} \left[\left\langle \sigma \left(\sum_m A_{nm} s_m(t) \right) | \vec{s}(t) \in \mathcal{S}(S) \right\rangle \right], \quad (4)$$

where we use $\langle \cdot \rangle$ to denote the average over all nodes n . A is a network with many nodes and a uniformly random structure, so we approximate the expectation over $\mathcal{S}(S)$ by assuming each $s_n(t)$ is 1 with probability S and 0 otherwise, independent of the other nodes. Since nodes differ in the number and type of their inputs, this assumption is valid only for large, homogeneous networks. Thus, each node will have, on average, $S\langle k \rangle(1 - \alpha)$ active excitatory inputs and $S\langle k \rangle\alpha$ active inhibitory inputs. To account for the variability in the number of such inputs for any particular node (due to both the degree distribution of a random network and the stochasticity of the process), letting $\mathcal{P}(\beta)$ be a Poisson random variable with mean β , we model the number of active excitatory inputs as $n_e = \mathcal{P}(S\langle k \rangle(1 - \alpha))$ and the number of active inhibitory inputs as $n_i = \mathcal{P}(S\langle k \rangle\alpha)$. We describe the total input to the transfer function using n_e and n_i draws from the link weight distribution. Replacing the argument of σ in Eq. (4), and taking the expectation over the distributions of n_e and n_i , as well as over the link weight distributions, we approximate

$$\Lambda(S) \approx S^{-1} \mathbb{E} \left[\sigma \left(\sum_{j=1}^{n_e} w_j - \sum_{k=1}^{n_i} w_k \right) \right], \quad (5)$$

where w_j and w_k are independent draws from the link weight distribution. Eq (5) may be used for any function $0 \leq \sigma \leq 1$.

Ceaseless dynamics are now explained by the shape of the branching function, as shown in Fig. 3A. Specifically, for small S , $\Lambda(S) > 1$, i.e., low activity levels tend to grow, thus preventing the dynamics from ceasing. The role of inhibition in this growth of low activity may be succinctly quantified as

$$\Lambda_0 \approx \frac{1 - \alpha}{1 - 2\alpha}, \quad (6)$$

where $\Lambda_0 = \lim_{S \rightarrow 0^+} \Lambda(S)$ (derived in SM).

For moderate values of S , $\Lambda(S) = 1$, placing the network in a critical state where activity tends to, on average, replicate itself. For large values of S , $\Lambda(S) < 1$, preventing very high activity levels. Comparing Fig. 3A with Fig. 2C, our model and theory are consistent with the empirical branching functions obtained from the monkey. Our choice of S^* for cascade detection was the lowest value of S for which $\Lambda(S) < 1.01$, thus accounting for differences in the dynamics of the model for different α and acknowledging that for low activity, dynamics are not expected to be critical since $\Lambda(S)$ is far from unity. Our results are robust to moderate increases in S^* (Figs. S2 and S2).

The reason that moderate S results in $\Lambda(S) \approx 1$, yet $\Lambda_0 > 1$, can be understood in the following way. For an inhibitory node to affect network dynamics, it must inhibit a node that has also received an excitatory input; without excitatory input, a node will remain inactive with or without the inhibitory input. When network activity is very low, the probability of receiving a single input is small, and the probability of receiving both an excitatory and an inhibitory input is negligible. Thus, as network activity approaches zero, the effect of inhibition wanes. Since the network is balanced for moderate activity levels, the waning of inhibition at low S shifts the excitation-inhibition balance toward excitation, explaining the tendency of network activity to avoid complete quiescence. On the other hand, to explain why $\Lambda(S)$ decreases as S increases, we note that when network activity is very high, some nodes receive input in excess of the minimum necessary input to fire with probability one, and so input is “wasted” by exciting nodes that would become excited anyway, shifting the excitation-inhibition balance toward inhibition.

Many recently studied models of criticality and neuronal avalanches have focused on the excitatory neural population, assuming that inhibition can be treated indirectly as a behind-the-scenes influence that reduces excitatory signal transmission [1, 4–7, 16]. In addition to the lack of inhibitory neurons, one unrealistic aspect of dynamics in these models is that, in spite of having unity branching function, activity dies out with probability one in the absence of external stimulus. In contrast, real cortex dynamics never come to a halt, which makes predictions from these models difficult to compare with experiments. The addition of inhibitory neurons in our model not only makes it more realistic, but also makes the dynamics ceaseless. Although here we show ceaselessness at critical-

ity, based on the mechanism and branching function analysis, we expect that inhibition would also lead to ceaselessness in networks that deviate from criticality, due persistence of the $\Lambda > 1$ regime. Ceaseless activity is also more comparable with *in vivo* cortex recordings. Indeed, we found good agreement when we compared our model and analytical predictions with data from awake monkeys, introducing the branching function as a new means to do so. We note that our results are the first to identify signatures of critical dynamics in the form of power-law avalanche size distributions based on spiking activity in the cortex of an awake animal (most previous studies have focused on local field potential recordings [1, 9, 31]), which contrasts with previous attempts [13, 14, 31]. Our results also reveal that the question of whether cortex dynamics are critical is likely to depend on the activity level of the network (S in our work).

Our findings suggest that internal cognitive processes that depend on intrinsically ongoing cortex activity (e.g. memory consolidation) may fundamentally depend on the existence of inhibitory neurons. Our results also have implications in networks outside the context of neuroscience, where ceaseless dynamics may or may not be beneficial. For example, critical dynamics have been studied in gene interaction networks [32], the internet [33], and spreading of epidemics through social networks [34]. In all these cases, our results highlight a counterintuitive, but important consequence of inhibitory nodes: they can result in ceaseless dynamics.

D.B.L. was supported by Award Number U54GM088558 from the National Institute Of General Medical Sciences. The content is solely the responsibility of the authors and does not necessarily represent the official views of the National Institute Of General Medical Sciences or the National Institutes of Health. S.Y. and D.P. were supported by the Intramural Research Program of the National Institute of Mental Health. E.O. was supported by ARO Grant No. W911NF-12-1-0101.

[1] J. M. Greenberg, B.D. Hassard, S. P. Hastings, *Bull. Amer. Math. Soc.* **84**(6): 1296, (1978).
 [2] P. Erola, A. Diaz-Guilera, S. Gomez, A. Arenas, *Networks and Heterogeneous Media*. **7**(3): 385–397, (2012).
 [3] B. Karrer, M. E. J. Newman, *Phys. Rev. E*, **84**(3): 036106 (2011).
 [4] O. Kinouchi, M. Copelli, *Nature Physics* **2**: 348–351, (2006).
 [5] D. B. Larremore, W. L. Shew, J. G. Restrepo, *Phys. Rev. Lett.* **106**: 058101 (2011).
 [6] D. B. Larremore, W. L. Shew, E. Ott, J. G. Restrepo, *Chaos*. **21**: 025117 (2011).
 [7] W. L. Shew, H. Yang, T. Petermann, R. Roy, D. Plenz, *J. Neurosci.* **29**: 15595–15600 (2009).
 [8] W. L. Shew, H. Yang, W. Yu, R. Roy, D. Plenz, *J. Neurosci.* **31**: 55–63 (2011).
 [9] T. Petermann *et al.*, *Proc. Natl Acad. Sci. USA* **106**: 15921–6 (2009).
 [10] J. M. Beggs, D. Plenz, *J. Neurosci.* **23**: 11167–77 (2003).
 [11] S. S. Poil, A. van Ooyen, K. Linkenkaer-Hansen, *Human Brain Mapping* **29**: 770–777, (2008).

[12] S. S. Poil, R. Hardstone, H. D. Mansvelder, K. Linkenkaer-Hansen, *J. Neurosci.* **32**(29): 9817–9823 (2012).
 [13] G. Hahn *et al.*, *J. Neurophys.* **104**(6), 3312–3322 (2010).
 [14] T. L. Ribeiro *et al.*, *PLoS ONE* **5**: e14129, (2010).
 [15] D. L. Meinecke, A. Peters, *J. Comp. Neurol.* **261**: 388–404 (1987).
 [16] C. Haldeman, J. M. Beggs, *Phys. Rev. Lett.* **94**: e058101, (2005).
 [17] F. W. Ohl, H. Scheich, W. J. Freeman, *Nature* **412**: 733–736 (2001).
 [18] C. M. Lewis, A. Baldassarre, G. Committeri, G. L. Romani, M. Corbetta, *Proc. Natl. Acad. Sci. USA* **106**: 17558–17563 (2009).
 [19] I. Timofeev, F. Grener, M. Bazhenov, T. J. Sejnowski, M. Steriade, *Cerebral Cortex* **10**: 1185–1199 (2000).
 [20] D. A. McCormick *et al.*, *Cerebral Cortex* **13**: 1219–1231 (2003).
 [21] M. Le Bon-Jego, R. Yuste, *Frontiers in Neuroscience* **1**: 123–9 (2007).
 [22] J. Hopfield, *Proc. Natl Acad. Sci. USA* **79**: 2554–2558 (1982).
 [23] D. J. Amit, *Modeling brain function—the world of attractor neural networks*. Cambridge University Press: Cambridge, (1989).
 [24] T. P. Vogels, K. Rajan, L. F. Abbott, *Ann Rev. Neurosci.* **28**: 357–376 (2005).
 [25] A. Kumar, S. Rotter, A. Aertsen, *Nature Rev. Neurosci.* **11**: 615–627, (2010).
 [26] F. Barbieri, N. Brunel, *Frontiers in neuroscience* **2**: 114, (2008).
 [27] A. Levina, J. M. Herrmann, T. Geisel, *Nature Physics* **3**: 857–860 (2007).
 [28] D. Millman, S. Mihalas, A. Kirkwood, E. Niebur, *Nature Physics* **6**: 801–805, (2010).
 [29] D. B. Larremore, M. Y. Carpenter, E. Ott, J. G. Restrepo, *Phys. Rev. E* **85**: 066131, (2012).
 [30] A. Clauset, C. R. Shalizi, M. E. J. Newman, *SIAM Review* **51**: 661–703 (2009).
 [31] N. Dehghani *et al.*, *Frontiers in Physiology* **3** (2012).
 [32] C. Torres-Sosa C, S. Huang, M. Aldana, *PLoS Comp. Biol.* **8**(9): e1002669, (2012).
 [33] R.V. Sole, S. Valverde, *Physica A* **289**: 595–605, (2001).
 [34] S. Davis *et al.*, *Nature* **454**: 634 (2008).

INHIBITION GUARANTEES CEASELESS CORTEX NETWORK DYNAMICS SUPPLEMENTARY MATERIAL

Materials and Methods: Monkey electrophysiology.

All experiments with Monkey 1 were carried out according to the guidelines of the NIH and the Animal Care and Use Committee of the NIMH. One adult female monkey (*Macaca mulatta*) was studied. As described previously [1], we recorded multi-site unit activity with 96 channel multi-electrode arrays (Blackrock Microsystems, 10x10 array with no corner electrodes, 400 μm inter-electrode spacing, 1 mm electrode penetration depth) chronically implanted in the arm representation region of premotor cortex. Multielectrode array implantation was carried out using methods that have been described previously [2, 3]. The recordings (30 min duration, 30 kHz sample rate) were made while the monkey was awake and not engaged by any task or controlled sensory stimulus. The signals were band pass filtered from 300 to 3000 Hz followed by spike detection and sorting. The results presented here are based on 65 well isolated single units. Recordings were done one week following array implantation surgery. To obtain single unit activity, manual spike sorting was performed with Plexon Offline Sorter. The first 3 principal components, peak-to-trough amplitude, and non-linear energy were the waveform features used for sorting. We adopted a strict definition of a single unit as follows: in a 2-D projection of at least 2 of the sorting features the unit must have a mean that is strongly different from the mean of noise waveforms ($p \leq 0.001$, multivariate ANOVA). If more than one unit was recorded from the same electrode, the difference between means of each unit was also required to be significant at this strict level ($p \leq 0.001$, multivariate ANOVA).

All experiments with Monkey 2 were carried out according to the guidelines of the NIH and the Animal Care and Use Committee of Duke University approved all procedures. An 8x8 array of monopolar tungsten electrodes (30 μm diameter, 1M Ω impedance; 1-mm inter-electrode spacing) was chronically implanted into the left primary motor cortex (leg representation) of an adult rhesus monkey (*Macaca mulatta*). Electrodes were placed 1.5 mm deep. Extracellularly recorded spiking activity was sampled at 40 kHz and band-pass filtered with a two-pole low-cut and a four-pole highcut filter at 0.4-8 kHz. Off-line unit discrimination was based on principal component analysis and spike-template matching.

Materials and Methods: Empirical branching functions.

To test the predictions of our model and analysis using experimental data we analyzed the data as follows to create an empirical branching function. First, spike times from many neurons were used to create a spike count time series. This step requires a choice of the duration of time ΔT in which spikes will be counted. For the data shown in Figure 2A, B, C, we used $\Delta T = 25$ ms for Monkey 1. And $\Delta T = 50$ ms for Monkey 2. The rationale for using two different values of ΔT is that the data from Monkey 2 may have potentially longer timescales due to larger inter-electrode spacing in the electrode arrays. After obtaining a spikecount time series $c(t)$, the empirical branching function was obtained by plotting every ratio $c(t+1)/c(t)$ versus $c(t)$ for all t . The plots in Figure 2 present the median as well as the upper and lower quartiles of these ratios for every value of $c(t)$. Finally, this empirical branching function was used to select a threshold for defining avalanches. The threshold was chosen close to the spike count below which the branching function rises above 1. Given this choice of threshold, avalanches were defined as discussed in the main text.

Given the different number of single units obtained from the two monkeys (65 units Monkey 1, 131 units Monkey 2), we decided to test the sensitivity of our results to changes in the number of available units. For this we used our model, where we can easily control the number of available units (Fig. S1). We next tested for sensitivity to our choice of time bin ΔT for the model (Fig. S1) and for the monkeys (Figs. S2, S3). Finally we tested for sensitivity to small changes in the spike count threshold used to define cascades (Figs. S2, S3). We found that our main conclusions are largely unchanged by these different parameter choices used to analyze the data shown in Figure 2 of the main text.

Derivation of lifetime scaling.

The lifetime of network activity changes as a function of number of nodes N , inhibitory fraction α , and mean degree $\langle k \rangle$, hereafter simply k for notational convenience. Our approach is to derive the functional scaling of activity lifetime τ by using a Fokker-Planck description, examining the distribution of an ensemble of system states to find those from which cessation of activity is likely.

We treat network activity S as following a random walk between $S = 0$ and $S = 1$, with a mean change of S per step equal to $(\Lambda(S) - 1)S$. To find the diffusion coefficient we imagine that at $t = t_0 - 1$ all systems in the ensemble have the same $S(t_0 - 1)$

and we ask what the ensemble variance $\langle (S - \langle S \rangle)^2 \rangle$ is at time t_0 , where $\langle \cdot \rangle$ denotes an ensemble average and $S = N^{-1} \sum_i s_i$. Assuming each s_i is independently 1 with probability S and 0 otherwise, we get

$$\begin{aligned}
2D &= \langle (S - \langle S \rangle)^2 \rangle = N^{-2} \left\langle \left(\sum_i (s_i - \langle S \rangle) \right)^2 \right\rangle \\
&= N^{-2} \sum_{i,j} \langle (s_i - \langle S \rangle) (s_j - \langle S \rangle) \rangle \\
&= N^{-2} \sum_{i,j} \delta_{i,j} \langle (s_i - \langle S \rangle)^2 \rangle \\
&= N^{-2} \sum_i [\langle s_i^2 \rangle - 2\langle s_i \rangle \langle S \rangle + \langle S \rangle^2] \\
&= N^{-1} (\langle S \rangle - \langle S \rangle^2) = \mathcal{O}(N^{-1}) \ll 1.
\end{aligned} \tag{S1}$$

where we have used $\langle s_i^2 \rangle = \langle s_i \rangle$ since $s_i = 0$ or 1 . Since $\langle (S - \langle S \rangle)^2 \rangle = \mathcal{O}(N^{-1})$, typically $(S - \langle S \rangle) \sim N^{-1/2}$, and thus we substitute $\langle S \rangle \approx S$, concluding that

$$D \approx S(1 - S)/2N. \tag{S2}$$

Having calculated the diffusion coefficient, we continue with a Fokker-Planck approach to calculate the flux of probability corresponding to the cessation of network dynamics. To study the cessation of activity, we need to determine the behavior of $\Lambda(S)$ for small values of S . To do this, we expand $\Lambda(S)$ to first order in S . The Poisson variables n_e and n_i in Eq. (5) will contribute to first order behavior for only $(n_e, n_i) \in \{(1, 0), (2, 0), (1, 1)\}$. Inserting these cases into Eq. (5) we get

$$\Lambda(S) \approx S^{-1} \mathbb{E} [\sigma(w)P(n_e = 1, n_i = 0) + \sigma(w_1 + w_2)P(n_e = 2, n_i = 0) + \sigma(w_1 - w_2)P(n_e = 1, n_i = 1)] \tag{S3}$$

By replacing the Poisson probabilities for these cases, we get

$$\Lambda(S) \approx S^{-1} \mathbb{E} \left[\sigma(w)kS(1 - \alpha)e^{-kS} + \sigma(w_1 + w_2)\frac{1}{2}k^2S^2(1 - \alpha)^2e^{-kS} + \sigma(w_1 - w_2)k^2S^2(1 - \alpha)\alpha e^{-kS} \right] \tag{S4}$$

We then expand each exponential to first order in S and assume w is uniform in $[0, 2\gamma]$ so that $\gamma = \mathbb{E}[w] = [k(1 - 2\alpha)]^{-1}$. Assuming that $k \gg 1$ so that $\mathbb{E}[w] \ll 1$, we have that $\mathbb{E}[\sigma(w)] = [k(1 - 2\alpha)]^{-1}$ and $\mathbb{E}[\sigma(w_1 + w_2)] = 2\mathbb{E}[w]$. By integration, $\mathbb{E}[w_1 - w_2] = \gamma/3 = [3k(1 - 2\alpha)]^{-1}$. Substituting, we get

$$\Lambda(S) - 1 \approx \frac{\alpha}{1 - 2\alpha} \left[1 - \frac{2}{3}kS(1 - \alpha) \right], \tag{S5}$$

and we find that for small S , $\Lambda(S) - 1 = (\Lambda_0 - 1) [1 - 2kS(1 - \alpha)/3]$. We assume that, in general, we have $\Lambda(S) - 1 = (\Lambda_0 - 1)f[kS(1 - \alpha)]$, where $f(0) = 1$, $f(x) \rightarrow 0$ for large $x \gg 1$. In addition, since Eq. S5 indicates that the initial decrease of f with S scales with $kS(1 - \alpha)$, for the purposes of estimating the scaling of lifetime τ with k and α , we tentatively take the function $f(x)$ to be independent of α . Furthermore, we presume that $\Lambda(S)$ approaches one far from $S = 0$ for $Sk \gg 1$. This is in accord with Fig. 3 which shows a plateau centered at $S = 1/2$ where $\Lambda(S) = 1$ and this plateau extends down to small S . Thus $f(x)$ is supposed to be one at $x = 0$ and to approach zero for large x .

Next, we use a Fokker-Planck description with diffusion coefficient $D(S) = S(1 - S)/(2N)$ and a ‘‘velocity’’ in S of $v_S = (\Lambda(S) - 1)S = (\Lambda_0 - 1)Sf[(1 - \alpha)kS]$ where v_S is motivated by $S(t + 1) = \Lambda(S(t))S(t)$ so $S(t + 1) - S(t) = [\Lambda(S(t)) - 1]S(t)$. The time-independent Fokker-Planck equation is

$$\frac{\partial}{\partial S} \left[(\Lambda_0 - 1)f[(1 - \alpha)kS] SP(S) \right] = \frac{\partial}{\partial S} \left[D(S) \frac{\partial P(S)}{\partial S} \right]. \tag{S6}$$

Since $\Lambda(S)$ is substantially above one for small S and substantially below one for S very near $S = 1$ (see Fig. 3), we anticipate that $P(S)$ will have the overall qualitative form shown in Fig. S4, and we now attempt to estimate $P(S)$ in the region $S \sim 1/k$.

For $S \ll 1$, $D(S) \sim S/2N$, and Eq. (S6) becomes

$$(\Lambda_0 - 1)f[(1 - \alpha)kS]SP(S) = \frac{S}{2N} \frac{\partial P(S)}{\partial S}. \quad (\text{S7})$$

Defining $\hat{S} = (1 - \alpha)kS$, we have

$$\left[\frac{2N}{k(1 - \alpha)} (\Lambda_0 - 1) \right] f(\hat{S})P(S) = \frac{\partial P(S)}{\partial \hat{S}}. \quad (\text{S8})$$

In order to solve this equation, we define $x(\hat{S}) = \int_{\hat{S}}^{1/2} f(\hat{S}')d\hat{S}'$ and let $\hat{P}(x(\hat{S})) = P(S)$ which gives

$$- \left[\frac{2N}{k(1 - \alpha)} (\Lambda_0 - 1) \right] \hat{P}(x) = \frac{\partial \hat{P}(x)}{\partial x} \quad (\text{S9})$$

which yields

$$P(S) = P_0 \exp \left\{ - \frac{2N(\Lambda_0 - 1)}{k(1 - \alpha)} x[(1 - \alpha)kS] \right\}. \quad (\text{S10})$$

where $P_0 \sim P(1/2)$ (cf. Fig. S4).

In order for activity to cease entirely, $S \sim \sqrt{\langle (S - \langle S \rangle)^2 \rangle} \approx \sqrt{S/N}$ which implies that $S \approx 1/N$. While in this case the Fokker-Planck description is at the border of its range of validity, we presume that we can still use it for the purpose of obtaining a rough scaling estimate. Therefore, we write

$$(\text{flux out}) \approx (\text{const.})P(1/N) = (\text{const.})P_0 \exp \left[- \frac{2N(\Lambda_0 - 1)}{k(1 - \alpha)} x \left(\frac{k}{N}(1 - \alpha) \right) \right]. \quad (\text{S11})$$

Since we are primarily interested in scaling for large system size, we assume that $k/N \ll 1$, so $x[(1 - \alpha)k/N] \approx x(0) = \text{constant}$, and thus

$$(\text{flux out}) \approx (\text{const.})P_0 \exp \left[- \frac{2N(\Lambda_0 - 1)}{k(1 - \alpha)} x(0) \right]. \quad (\text{S12})$$

We now estimate $\tau = (\text{total probability})/(\text{probability flux out})$, and substitute the definition of $\Lambda_0 - 1 = \alpha/(1 - 2\alpha)$, yielding

$$\tau = C_1 \exp \left[C_2 \left(\frac{N\alpha}{k(1 - \alpha)(1 - 2\alpha)} \right) \right] \quad (\text{S13})$$

and we therefore argue that lifetime τ scales with a single scaling parameter $q = (N/k) [\alpha/(1 - \alpha)(1 - 2\alpha)]$, as

$$\tau(q) = C_1 \exp [C_2 q]. \quad (\text{S14})$$

Derivation of Λ_0 .

To better understand the tendency for low activity to grow, we investigate $\Lambda_0 = \lim_{S \rightarrow 0^+} \Lambda(S)$. This limiting case will consist of a single active node. A single active inhibitory node will produce zero additional active nodes, so the calculation of Λ_0 simplifies considerably. Thus we let $n_e = 1$ and $n_i = 0$ in Eq. (5), and substitute in the Poisson probability, in which case the limit simplifies to $\Lambda_0 = E[\sigma(w)] \langle k \rangle (1 - \alpha)$, where w is a draw from the link weight distribution. This expression has the following intuitive interpretation: the expected number of activated nodes immediately following a single active node is equal to the product of (i) the expected value of the transfer function after receiving a single excitatory input, (ii) the mean degree $\langle k \rangle$, and (iii) the probability that the single active node is excitatory. For the simple piecewise linear σ , and assuming $0 \leq w \leq 1$, we get $\Lambda_0 = \gamma \langle k \rangle (1 - \alpha)$. Furthermore, since $\gamma \approx 1/[\langle k \rangle (1 - 2\alpha)]$, we conclude that

$$\Lambda_0 \approx \frac{1 - \alpha}{1 - 2\alpha}. \quad (\text{S15})$$

| Data | Avalanche size distribution exponent |
|---------------------------------|--------------------------------------|
| $\alpha = 0.0$ | 1.50 |
| 0.10 | 1.48 |
| 0.15 | 1.47 |
| 0.20 | 1.48 |
| 0.25 | 1.47 |
| 0.30 | 1.47 |
| Monkey 1 | 1.54 |
| Monkey 2 | 1.52 |
| Subsampled Model $\alpha = 0.2$ | 1.58 |

TABLE S1. Power-law exponents were calculated using maximum likelihood methods [30].

Note that Λ_0 is only a function of the fraction of inhibitory nodes, and does not depend on the total number of nodes or mean degree. The factor $(1 - \alpha)$ in the numerator of (S15) reflects the fact that only excitatory nodes contribute to Λ_0 .

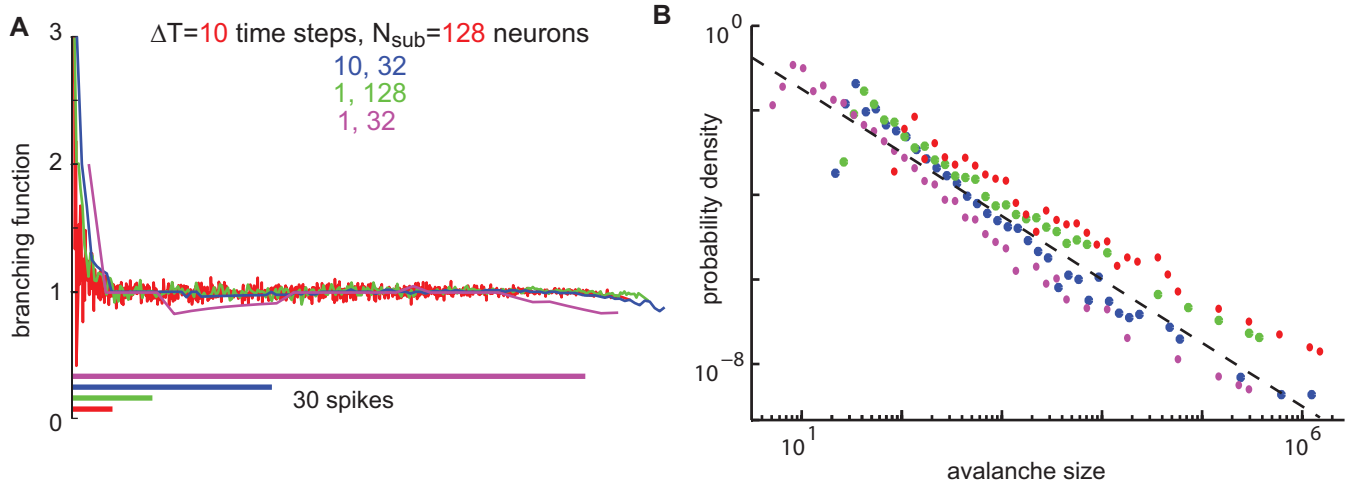


FIG. S1. **Robustness to undersampling and choices of ΔT .** **A**) Four empirical branching functions from the same model data that was analyzed in Figure 2 of the main text. The shape of the branching function is largely robust to choices of ΔT (red and blue - 10 timesteps; green and purple - 1 timestep) and to different degrees of subsampling (red and green - $N_{sub} = 128$ neurons; blue and purple - $N_{sub} = 32$ neurons). Note that the horizontal axis (spike count) is scaled from 0 to the maximum possible spike count, $N_{sub}\Delta T$, as indicated by the colored scale bars. **B**) The avalanche size distributions corresponding to the same ΔT and N_{sub} conditions as in A. Notice that there are slight differences among these distributions, but the overall conclusion that they are close to power-law in functional form is not very sensitive to changes in ΔT and N_{sub} . Black dashed line is a -1.5 power-law. Color code matches that in A.

[1] W. L. Shew, H. Yang, W. Yu, R. Roy, D. Plenz, *J. Neurosci.* **31**: 55–63 (2011).

[2] S. Suner *et al.* *IEEE Trans Neural Syst Rehabil Eng* **13**: 524–541 (2005).

[3] M. A. Nicolelis *et al.* *Proc Natl Acad Sci USA* **100**: 11041–11046 (2003).

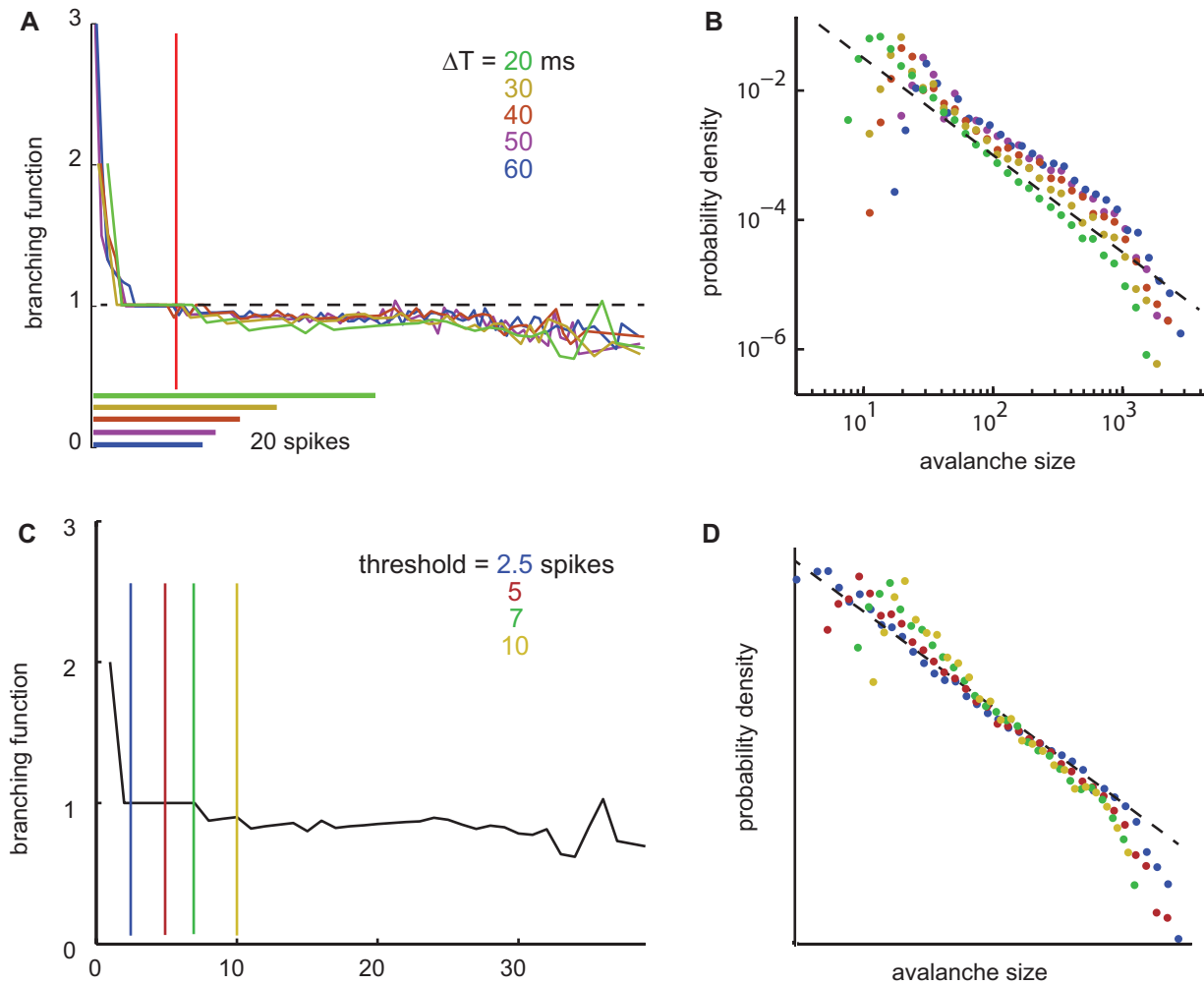


FIG. S2. Monkey 1: Robustness to choices of ΔT and cascade threshold. **A)** Five empirical branching functions from the Monkey 1 data that was analyzed in Figure 2 of the main text. Notice that the shape of the branching function is largely unchanged for different choices of ΔT (green - 20 ms, gold - 30, red - 40, purple - 50, blue - 60). The horizontal axis (spike count) is scaled by ΔT to account for different maximum possible spike counts for different ΔT values, as indicated by the colored scale bars. The red line indicates the threshold used to create the avalanche size distributions in panel B. **B)** The avalanche size distributions corresponding to the same ΔT conditions as in A. Notice that there are slight differences among these distributions, but the overall conclusion that they are close to power-law in functional form is not very sensitive to changes in ΔT . Black dashed line is a -1.5 power-law. Color code matches that in A. **C)** Empirical branching function for $\Delta T = 20$ ms. The vertical colored lines indicate different thresholds used to create the avalanche size distributions shown in panel D. **D)** Avalanche size distributions corresponding to the thresholds shown in panel C. Notice that there are slight differences among these distributions, but the overall conclusion that they are close to power-law in functional form is not very sensitive to changes in threshold. Black dashed line is a -1.5 power-law. Color code matches that in C.

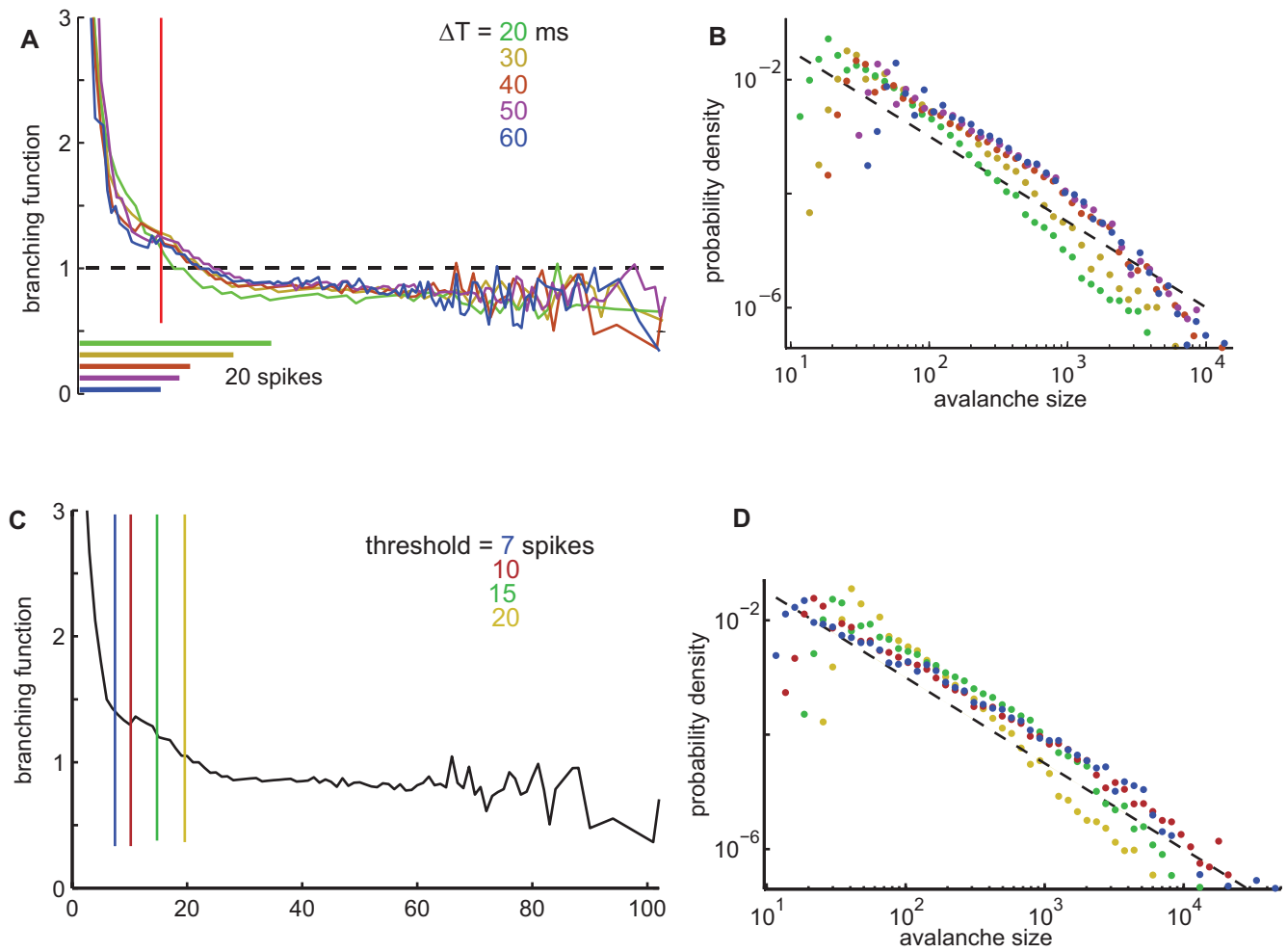


FIG. S3. **Monkey 2: Robustness to choices of ΔT and cascade threshold.** A-D) Same caption as for Fig. S3 except for the following. Different color codes as indicated. The empirical branching function in C was constructed with $\Delta T = 40$ ms.

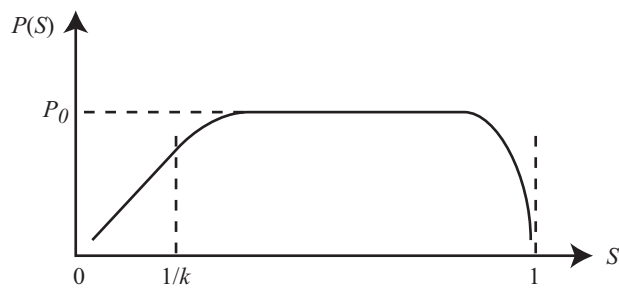


FIG. S4. **Form of $P(S)$.**